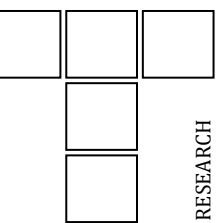


Vol. 47, No. 2 (2025) 389-400, DOI: 10.24874/ti.1947.04.25.06

Tribology in Industry

www.tribology.rs



Functional Surfaces Roughness Analysis of 3D Printed PET-G Housings Used for Press-Fitting Steel Ball Bearings

Živana Jovanović Pešić^a, Nenad Petrović^a, Strahinja Milenković^b, Nenad Kostić^a, Dragan Džunić^{a,*}

^aUniversity of Kragujevac, Faculty of Engineering, Sestre Janjić 6, 34000 Kragujevac, Serbia, ^bUniversity of Kragujevac, Institute for Information Technologies, Jovana Cvijića bb, 34000 Kragujevac, Serbia.

Keywords:

Surfaces roughness Profilometry Press fit Pulling out 3D printing PET-G

* Corresponding author:

Dragan Džunić E-mail: dzuna@kg.ac.rs

Received: 6 April 2025 Revised: 12 May 2025 Accepted: 2 June 2025



ABSTRACT

The study examines the impact of mechanical loading on the surface integrity and retention performance of press-fit joints in polymer housings produced by additive manufacturing. Components were fabricated using a thermoplastic material and subjected to controlled assembly and disassembly processes of steel ball bearings. Surface roughness was measured before and after press-fitting to evaluate the effects of mechanical contact. Force-displacement curves were recorded during both insertion and extraction to quantify retention behavior. Three groups of samples were tested: unassembled reference parts, samples with one assembly cycle, and samples with two cycles. Results indicate a reduction in surface roughness and press-fit resistance with repeated cycles. The second insertion in samples exposed to two cycles resulted in a significant decrease in required force compared to the first. Similarly, surface roughness values decreased, suggesting plastic deformation and material wear. The findings confirm that repeated mechanical loading degrades surface texture and weakens the retention capacity of the joint. This study emphasizes the importance of accounting for material behavior under repeated stress in the design of interference-fit assemblies produced by additive manufacturing.

© 2025 Published by Faculty of Engineering

1. INTRODUCTION

Polyethylene Terephthalate Glycol (PET-G) is a widely used thermoplastic polymer known for its excellent balance of mechanical strength [1], durability, and ease of processing. One of its key advantages is its high impact resistance, which

makes it a preferred material for applications requiring durability and toughness. Additionally, PET-G exhibits good chemical resistance, enabling it to withstand exposure to various chemicals without significant degradation [2]. Unlike its predecessor, polyethylene terephthalate (PET), PET-G is modified with

glycol, which enhances its clarity, improves flexibility, and reduces brittleness. modification yields a material that is easier to process and less prone to cracking under stress, making it particularly well-suited for applications requiring durability and strength [3]. Its low shrinkage and minimal warping during processing further enhance its suitability for 3D printing, ensuring high dimensional accuracy and consistent print quality [4]. These properties, combined with its transparency, flexibility, and recyclability [5], contribute to its growing popularity in industries such as manufacturing, packaging, and medical applications, where both mechanical performance and aesthetic qualities are essential.

PET-G material exhibits significantly lower susceptibility warping compared to Acrylonitrile Butadiene Styrene (ABS), making it a more stable option for 3D printing applications [6]. One of its key advantages is its ability to print at lower temperatures, which not only reduces the risk of thermal distortion but also minimizes energy consumption during the printing process. Additionally, PET-G demonstrates excellent layer adhesion, resulting in strong and durable printed objects with fewer structural weaknesses. Numerous studies [7-9] have explored various parameters and phenomena associated with 3Dprinted parts, highlighting the significant potential of this field. Unlike some other thermoplastics, it produces minimal odor during printing, making it a more user-friendly material, especially for indoor environments. These properties, along with its balance of strength, flexibility, and ease of use, make PET-G a preferred choice for both professional and hobbyist 3D printing applications, ranging from prototypes and functional parts to decorative and consumer-grade products.

Given its favorable combination of mechanical properties, PET-G is increasingly being explored in applications that require precise mechanical assembly, such as press fitting. Press fitting represents a widely adopted assembly technique that enables the joining of components without the use of adhesives, threaded fasteners, or welding processes. Instead, mechanical interference is employed by applying pressure to one component so that it fits tightly within or over another, forming a reliable and structurally sound joint. This method offers several benefits,

including reduced assembly time, cost efficiency, and improved performance due to the absence of stress concentrations typical of other joining methods.

The success of press-fitted joints depends heavily on the material's strength, dimensional stability, and surface characteristics—areas in which PET-G shows considerable promise. Its low shrinkage during 3D printing, combined with excellent dimensional accuracy and strong layer adhesion, makes it well-suited for producing components with the tight tolerances required for effective interference fits. Additionally, its good impact resistance and flexibility help absorb assembly stresses without cracking, thereby ensuring long-term structural integrity.

In a study conducted by Rashed et al. [10], the deformation behavior and geometric deviations resulting from press-fitting a thick-walled cylindrical component into a square housing were analyzed using finite element analysis (FEA). Such studies underscore the importance of understanding stress distribution and shape evolution during press-fit assembly. Press fitting is widely utilized in industries such as automotive [11], railway [12], hydraulic and pneumatic systems, metal fabrication, and the medical sector [13,14], and its integration with 3D-printed thermoplastics like PET-G may further expand the versatility and costeffectiveness of additive manufacturing technologies.

Surface quality is a critical factor influencing the mechanical performance and functionality of 3Dprinted components, particularly when these components are intended for assemblies involving press-fitting standard ball bearings. Surface roughness, in particular, affects contact behavior, stress distribution, and wear resistance during the service life of such assemblies [15]. In the context of press-fitting ball bearings into 3Dprinted PET-G housings, the precision and quality of the mating surface are paramount. The layerby-layer nature of fused deposition modeling (FDM) inherently results in anisotropic surface textures, which can vary depending on printing parameters such as layer height, extrusion width, nozzle temperature, and print speed [16,17]. These parameters significantly influence the surface roughness and, consequently, performance of the press-fit assembly. Therefore, accurate measurement and analysis of surface roughness are essential for predicting the performance of such hybrid assemblies. Several studies have investigated the impact of additive manufacturing parameters on the surface roughness and dimensional accuracy of thermoplastic components, particularly those made from PET-G [15,16,18]. However, limited research has focused on surface characterization in functionally assembled parts such as bearing housings.

This study aims to address that lack of information by evaluating the surface roughness of PET-G components designed for press-fit applications with standard, steel ball bearings, with the goal of understanding the influence of surface texture on fit integrity and potential performance in real-world use.

2. SAMPLE PREPARATION

2.1 Samples for press-fitting

The samples were designed using CATIA V5 R21, and exported in STL format with a sag tolerance of 0.2 mm, ensuring sufficient resolution for accurate surface geometry representation (Figure 1-a). The models consisted of square blocks with central circular holes designed to house ball bearings via press fitting. Based on the results from [19], the selected sample diameter was 25.8 mm for a 608 bearing with an outer diameter of 26 mm. These bearings were chosen due to their widespread use in hobbyist applications and the 3D printing community.

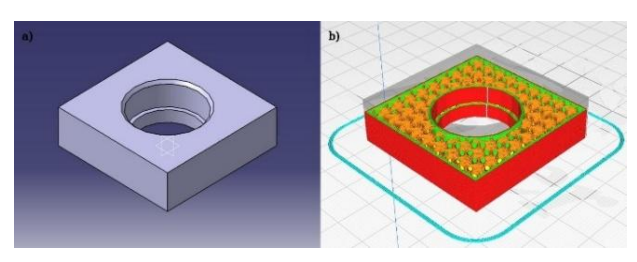


Fig. 1. a) CAD model of the bearing seat designed in CATIA V5 R21 and b) preview of the sliced model in Ultimaker CURA 4.11.0 prior to 3D printing.

The slicing process was performed using Ultimaker CURA 4.11.0, as shown in Figure 1-b, applying the parameters listed in Table 1. All samples were printed using a commercially available Creality Ender 3 printer equipped with

silent motor drivers, a dual-gear extruder, and a G10 build plate. The filament used was DevilDesign PET-G (purple) with a diameter of 1.75 mm. Printing was carried out under controlled conditions, with a room temperature of 25 °C and relative humidity of 40%. The average build time per bearing seat was approximately 1 hour and 15 minutes.

Table 1. 3D printing parameters.

Parameters	Values
Layer height	0.2 mm
Wall line count	3
Top/Bottom layer count	3
Z-seam alignment	Random
Printing temperature	235°C
Bed temperature	75℃
Infill density	20%
Infill pattern	Gyroid

The 3D printing parameters are summarized in Table 1, while Figure 2 shows the fabricated sample. All parameters not listed in table 1 are default slicer values for the used printer.



Fig. 2. 3D printed sample.

2.2 Sample for surface roughness measurement before press-fitting

To evaluate the surface roughness of the inner surface of the bearing seat before press-fitting, a simplified test sample was designed. This sample represents one-half of the complete geometry used for the actual press-fitting of the bearing. By isolating and exposing the internal cylindrical surface, the sample enables direct and unobstructed access for surface characterization. This approach eliminates the influence of assembly-induced deformations ensuring that the measurements accurately reflect the surface quality resulting solely from the 3D printing process. The geometry was modeled using CATIA V5 R21, maintaining the same dimensional features as the functional part but cut along the mid-plane to expose the interior of the seat.

The generated CAD model (Fig 3-a) was then processed in Ultimaker CURA 4.11.0 (Fig 3-b), using identical printing parameters presented in Table 1, in order to ensure consistency in print quality and surface finish. The sample (Fig 3-c) was printed using the same material-DevilDesign PET-G (purple)-and under the same controlled environmental and machine settings. This consistency enables meaningful comparison between the measured roughness values and the surface behaviour observed during the press-fit process. The prepared sample provides a reliable reference for evaluating how the initial surface state may influence mechanical fit and functional performance after assembly.

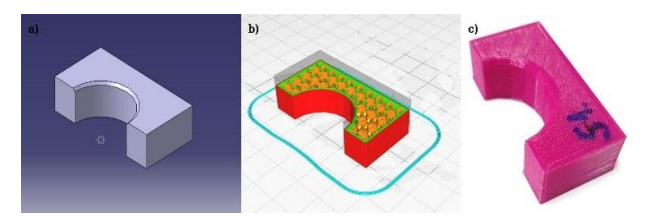


Fig. 3. a) CAD model of the bearing seat designed in CATIA V5 R21, b) preview of the sliced model in Ultimaker CURA 4.11.0 prior to 3D printing and c) 3D printed sample.

Table 2 provides an overview of the three experimental groups used in the study. Group 1 serves as the control group with no mechanical interaction, while Groups 2 and 3 were subjected to one and two full assembly-disassembly cycles, respectively. Each group consisted of three individual samples to ensure repeatability and statistical relevance of the measurements.

Table 2. Overview of sample groups and number of press-fitting/pulling-out cycles.

Sample Group	Description	Number of Cycles (Press-Fit + Pull-Out)	Number of Samples
Group 1	Reference samples - no press-fitting or pulling-out	0+0	3
Group 2	One press-fitting followed by one pulling-out	1+1	3
Group 3	Two press-fittings and two pulling-outs (repeated assembly cycles)	2+2	3

3. EXPERIMENTAL SETUP FOR PRESS-FITTING AND PULLING-OUT

To investigate the mechanical response of 3D-printed PET-G components during both the assembly (press-fitting) and disassembly (pulling-out) of standard ball bearings, a controlled experimental setup was developed. The primary objective was to replicate practical assembly conditions under well-defined and repeatable loading scenarios. The experimental approach was designed to simulate interference-fit situations, where a bearing is inserted into a slightly undersized 3D-printed housing by applying a controlled axial force. Likewise, the extraction of the bearing was carried out by applying an opposite axial force in order to remove the bearing from the housing.

The setup included the use of the Brookfield CT3-50kg Texture Analyser, an advanced device capable of applying and precisely measuring forces up to 50 kg (5000 N). The analyser offers high-resolution force and displacement tracking, with a load resolution of 5 g, a step resolution of 0.1 mm, and an accuracy of 0.1 mm, making it suitable for detailed evaluation of press-fit

phenomena. During testing, force and displacement data were continuously recorded in real-time, allowing for immediate digital analysis of the interaction between the bearing and the printed housing. This ensured accurate tracking of force as a function of insertion depth, enabling identification of force peaks related to tight fits or surface inconsistencies.

Each 3D-printed bearing housing was tested individually. Insertion and extraction were carried out slowly, at a constant speed, to avoid dynamic effects or shock loading. Custom-made alignment tools and holding fixtures were used to maintain axial symmetry and prevent misalignment during both press-fitting and pulling-out. The results were used to evaluate the fit quality and identify optimal interference values based on force trends and surface integrity after each operation.

A schematic representation of the experimental setup is shown in Figure 4, where (a) illustrates the press-fitting phase and (b) the pulling-out procedure. These diagrams illustrate the direction of applied force and the position of the bearing relative to the printed housing during each stage of testing.

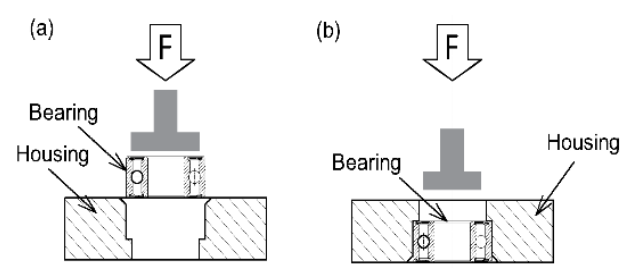


Fig. 4. Schematic representation of the experimental setup for (a) press-fitting and (b) pulling out of the bearing into/from the 3D-printed housing.

In this study, groups two and three of samples were used to investigate the effects of repeated mechanical loading on the 3D-printed bearing housings. The second group consisted of samples in which a standard ball bearing was press-fitted once and then pulled out once, simulating a single assembly-disassembly cycle. This procedure was repeated on three separate samples to ensure consistency and reproducibility. The third group included samples subjected to two complete cycles, where the bearing was press-fitted, pulled out, then press-fitted again and finally pulled out. This group also consisted of three samples, each experiencing two full loading-unloading sequences. The purpose of using these two groups was to evaluate the potential cumulative effect of repeated press-fitting and extraction on the surface condition and structural integrity of the PET-G housings.

4. SURFACE ROUGHNESS CHARACTERIZATION OF 3D-PRINTED SAMPLES

Surface topography plays a critical role in the functional behaviour of mechanical assemblies, especially those involving press-fit joints, where the quality of contact surfaces directly influences frictional resistance and mechanical stability. Accurate roughness measurement allows for the assessment of surface quality and its potential impact on wear, deformation, and fit precision. As emphasized by Gadelmawla et al. [20] and Bhushan [21], the selection of appropriate roughness parameters measurement methods is essential for reliable surface evaluation, particularly in the context materials processed additive by manufacturing techniques.

The surface roughness analysis was conducted using the INSIZE ISR C-002 profilometer (Figure 5), which enables precise determination of roughness parameters through a contact measurement method. The profilometer uses a stylus-based system to trace the surface profile along a defined path, recording vertical deviations from a mean line to calculate common roughness metrics such as Ra and Rz. These parameters were evaluated in accordance with ISO 4287, which defines profile-based surface roughness evaluation using stylus methods. The measurements were performed in the axial direction, parallel to the layer lines of the 3D-printed surface, in order to capture the texture most relevant to press-fit loading and sliding interactions. The reference measurement length was set to 4 mm for Group 1 samples, while a shorter path of 1.5 mm was used for Groups 2 and 3 to focus on the regions affected by contact during mechanical loading. The reduced length visible in the diagrams is a result of Gaussian filtering and data selection performed by the profilometer software to emphasize the central segment of the measured profile.

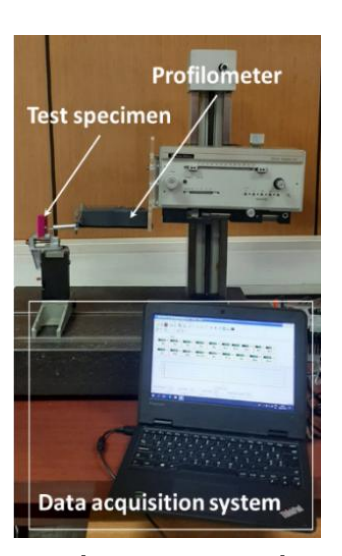


Fig. 5. Surface roughness testing on the profilometer.

Figure 5 also schematically illustrates the measurement configuration. For each group of samples, three independent measurements were carried out to ensure the repeatability and consistency of the data. This structure enabled the evaluation of how repeated pressfitting and extraction influence the inner surface quality of the printed bearing seats.

5. RESULTS AND DISCUSSION

The results obtained from surface roughness measurements and press-fitting force analysis are presented and discussed in this section. The primary objective was to evaluate the impact of mechanical loading-specifically press-fitting and pulling out-on the inner surface quality and mechanical performance of 3D-printed PET-G housings. Three distinct groups of samples were analyzed: unassembled reference parts, samples subjected to one press-fit and removal cycle, and samples exposed to two complete assembly-disassembly sequences.

The appearance of the press-fitted assembly, highlighting the final positioning and alignment of the bearings within the housing, is shown in Figure 6. This visual representation provides insight into the quality and precision of the press-fitting process.



Fig. 6. Final appearance of the press-fitted bearing within the 3D-printed PET-G housing, illustrating proper alignment and seating of the component after assembly.

5.1 Press-fitting and pulling-out

Figure 7 shows the average force-displacement curve for Group 2 samples, each of which underwent a single press-fitting and pulling-out cycle. The plotted data represent the mean of three independent measurements, ensuring consistency and repeatability.

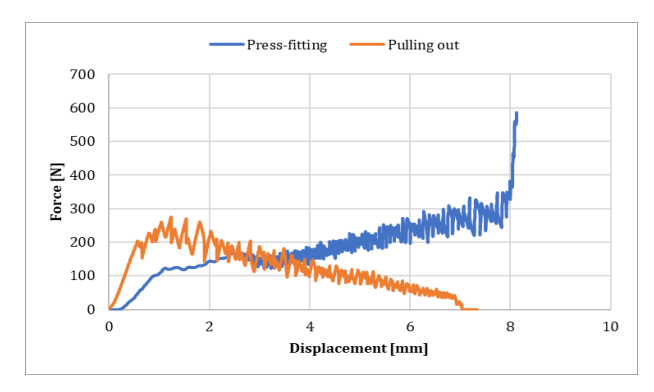


Fig. 7. Average force-displacement curve for pressfitting and pulling-out of Group 2 samples (n = 3).

The press-fitting phase exhibits a steady increase in force as the bearing enters the housing, reaching a peak of approximately 600 N, indicating a strong interference fit. The gradual rise in force reflects progressive contact and increasing resistance due to dimensional mismatch. This behaviour corresponds well with previous findings by You et al. [22], where the press-fitting process was divided into three stages: initial, stable, and final, with the stable stage exhibiting a near-linear increase in force as displacement increases. The authors also emphasized that deviations from ideal press-fit curves can be attributed to factors such as surface roughness, geometric tolerances, and elastic deformation at the contact interface. The pullingout phase starts with a peak just above 300 N, followed by a decreasing trend as the bearing is gradually extracted. Oscillations observed during extraction are attributed to stick-slip behaviour and localized surface interactions. These results confirm that, even after one complete cycle, the press-fit remains mechanically stable with no significant reduction in holding force.

Figure 8 presents the average force-displacement curves for Group 3 samples, each subjected to two consecutive press-fitting and pulling-out cycles. The results are shown separately for the first and second insertions (blue and purple curves) and the first and second removal (orange and black curves), respectively.

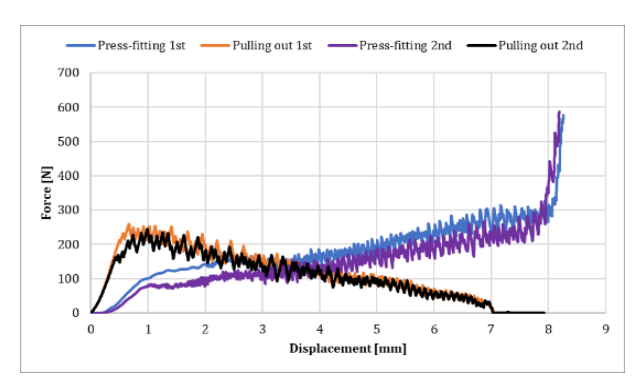


Fig. 8. Average force-displacement curves for two consecutive press-fitting and pulling-out cycles in Group 3 samples.

In the first press-fitting cycle, the force gradually increases to approximately 600 N, consistent with Group 2, indicating strong initial interference. During the first pulling out, a peak force slightly above 300 N is observed, followed by a steady decline, mirroring the behaviour noted in Group 2.

However, during the second press-fitting, a noticeable reduction in resistance is observed throughout the curve, with the maximum force reduced to around 400 N. This decrease indicates a weakening of the interference due to surface wear, plastic deformation, or slight dimensional enlargement of the housing. The second pulling out follows the same trend, with a lower peak force and less variation, suggesting smoother extraction and diminished contact friction.

These results confirm that repeated press-fitting and removal cycles negatively affect the press-fit quality by reducing retention forces, which may compromise long-term stability and dimensional integrity of the housing. This trend aligns with the findings of Dieudonné et al. [23], demonstrated that both insertion and disassembly forces in press-fit joints decrease progressively with successive assembly-disassembly operations, even in the absence of additional surface treatment or vibration assistance.

5.2 Surface Roughness Results

This section presents the results of surface roughness measurements conducted on all three sample groups: the reference samples without any mechanical loading (Group 1), the samples that underwent a single press-fitting and pulling-out cycle (Group 2), and those exposed to two complete cycles (Group 3). Each sample was measured three times to ensure repeatability and statistical relevance. The arithmetic average roughness (Ra) is defined as the average absolute deviation of the roughness profile from the mean line, and is calculated as follows:

$$Ra = \frac{1}{L} \int_0^L |z(x)| dx \tag{1}$$

where L is the evaluation length and z(x) represents the height of the surface profile at position x. The primary goal was to evaluate how mechanical contact between the bearing and the printed PET-G surface affects surface texture and roughness parameters, particularly after repeated loading.

The average surface roughness values (R_a) and maximum profile height (R_z) were calculated for each group and presented in Figure 9. Group 2 showed slightly reduced Ra values compared to Group 1, indicating potential plastic deformation

or surface compression after a single mechanical cycle, consistent with prior observations of contact-induced surface flattening in thermoplastics [24]. The average R_a across all Group 2 samples was 13.8 μm , which is approximately 6.8% lower than the average of Group 1. In contrast, Group 3 showed more variable roughness values, with an average Ra of 13.2 μm , marking a reduction of about 10.8% relative to Group 1.

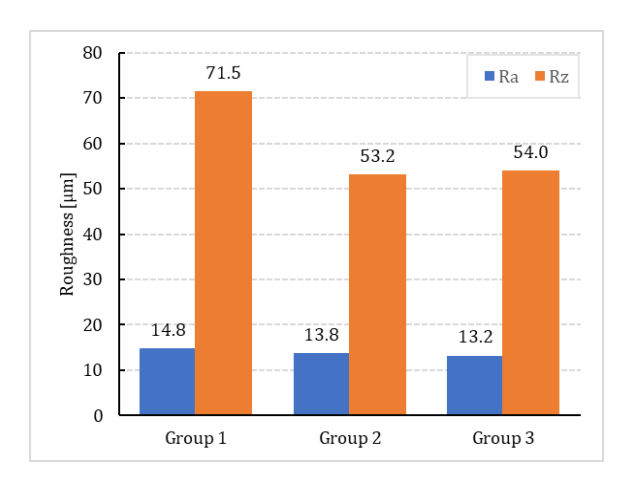


Fig. 9. Average surface roughness parameters R_{a} and R_{z} for each group.

The R_z values also followed a similar trend. Group 2 exhibited a mean R_z of 53.2 μm , while Group 3 showed a mean value of 54.00 μm , both significantly lower than the Group 1 average of 71.5 μm . This suggests that repeated mechanical cycling causes a partial smoothing of surface peaks, likely due to material yielding and surface abrasion during the press-fit and removal processes.

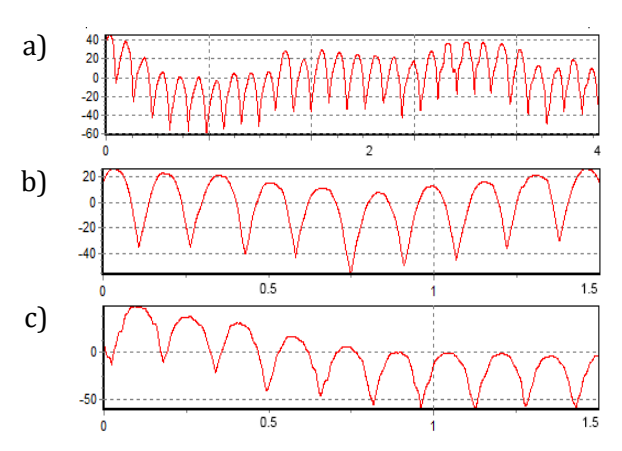


Fig. 10. Raw surface profiles.

Raw surface profiles are presented in Figure 10 to provide a direct visual insight into the actual surface morphology of the samples. Each trace

represents one typical unprocessed profile from each group: Group 1 (Figure 10-a), Group 2 (Figure 10-b), and Group 3 (Figure 10-c). These profiles clearly reveal differences in peak rounding, waviness, and local deformation.

Figure 11 shows the surface roughness profiles of three representative samples from Group 1, which were not subjected to any mechanical loading. The curves illustrate the characteristic topography of 3D-printed PET-G parts produced using FDM technology, where the layered deposition leads to periodic surface undulations along the measurement path.

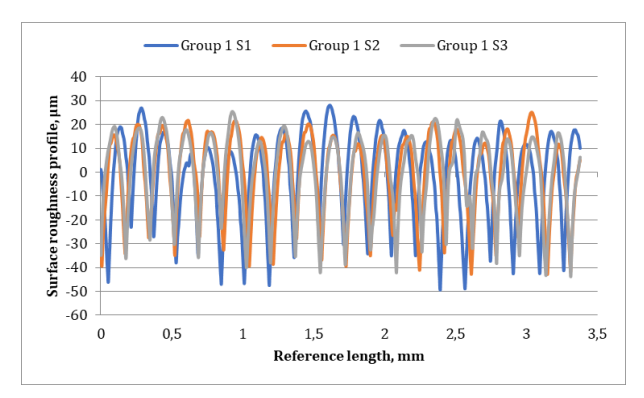


Fig. 11. Surface roughness profiles of unassembled reference samples.

The amplitude of the peaks and valleys remains relatively consistent across all three samples, indicating a uniform and reproducible surface texture resulting from the selected printing parameters. The roughness profiles exhibit regular wave-like patterns, with peak heights ranging from approximately +30 μm to -50 μm , which is typical for extruded thermoplastics printed with a 0.2 mm layer height. These results serve as a baseline reference for evaluating the impact of mechanical contact in Groups 2 and 3.

Figure 12 presents the variation of the maximum profile height (R_{max}) along the normalized reference length for three unloaded reference samples (Group 1). The curves show a consistent downward trend. reflecting the distribution of surface irregularities produced during the FDM printing process. The initial values of R_{max} range between 65 and 75 μ m, with sample S1 showing slightly higher values than S2 and S3 across most of the profile. This suggests minor variability in the height of surface peaks, which is expected due to thermal gradients and deposition path variation in FDM-printed parts.

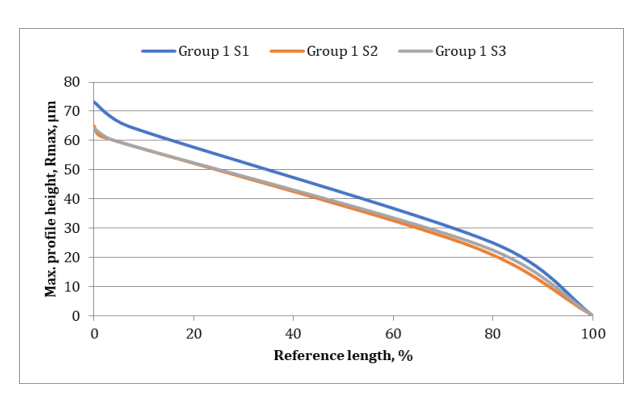


Fig. 12. Maximum profile height (R_{max}) distribution over reference length for Group 1 samples.

As the reference length increases, the R_{max} values steadily decrease for all three samples, converging toward zero. This behaviour is typical of rough surfaces where occasional high peaks dominate the early portion of the length but are less frequent across the full profile. The consistency of the curves supports the repeatability of the printing process under controlled conditions and establishes a reliable baseline for comparison with mechanically loaded samples.

Figures 13 presents the average surface roughness profiles for three individual samples (S1-S3) from Group 2, each of which underwent a single press-fitting and pulling out cycle. The profiles demonstrate significant differences compared to the unassembled reference samples from Group 1, particularly in terms of amplitude and waveform regularity.

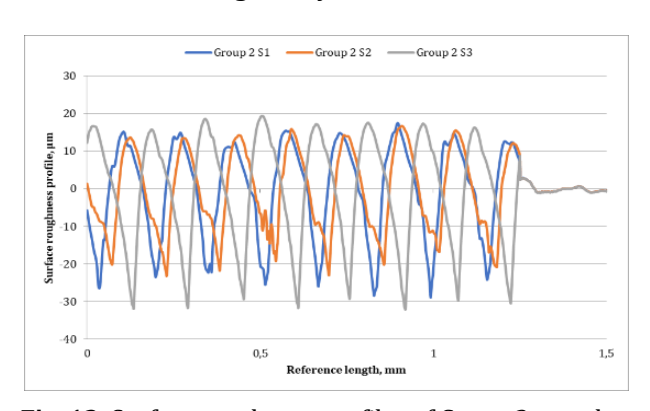


Fig. 13. Surface roughness profiles of Group 2 samples.

Sample S1 shows moderately regular peaks and valleys but with some noticeable asymmetry and variation in amplitude. This suggests localized deformation or material displacement along the surface due to mechanical contact during assembly and disassembly. The peak heights

reach approximately +15 μm, while valleys extend to around -30 µm. Sample S2 displays a more compressed and irregular pattern, with peaks mostly below +15 µm and valleys around -20 µm. The profile is less uniform than that of S1, indicating increased surface disruption, possibly caused by uneven pressure or microabrasion during bearing insertion and removal. Sample S3 exhibits the most uniform wave-like profile of the three, with peaks and valleys appearing at regular intervals and reaching similar amplitude values as in S2. Despite the mechanical interaction, the profile appears relatively stable, suggesting that some areas may be more resistant to deformation due to favorable orientation or local reinforcement in the printed structure.

Figure 14 shows the R_{max} distribution over normalized reference length for all three Group 2 samples (S1-S3), which were subjected to one complete press-fitting and pulling out cycle. Compared to the reference samples in Group 1, the curves here exhibit a notable reduction in initial peak values and a more gradual decline along the reference length.

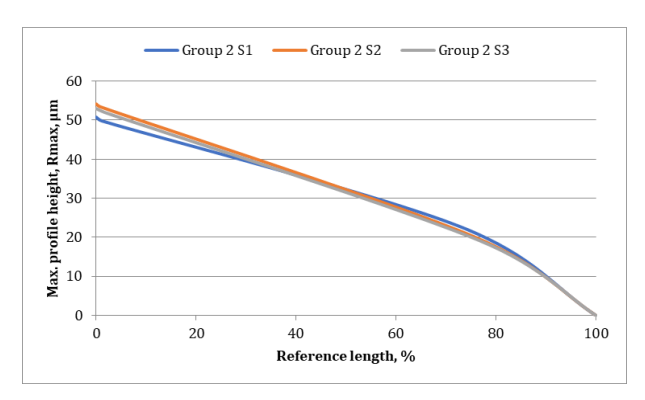


Fig. 14. Maximum profile height (R_{max}) distribution over reference length for Group 2 samples.

Sample S1 begins with the lowest initial R_{max} value (approximately 50 μ m) and exhibits a smooth, steady decay toward zero. This suggests moderate peak flattening and surface smoothing, likely caused by uniform mechanical contact during assembly. Sample S2 shows a slightly higher initial R_{max} (approx. 54-55 μ m), but follows a similar linear downward trend. The elevated start may reflect isolated surface asperities that remained after press-fitting, while the consistent slope suggests that those features were progressively levelled during removal. Sample S3 starts near 53 μ m but exhibits a sharper drop-off

after the 70% reference length mark. This could indicate localized deformation or partial tearing near the end of the profile, possibly due to frictional stress concentrations during disassembly.

Figure 15 shows the surface roughness profiles for Group 3 samples (S1-S3), which underwent two complete press-fitting and pulling-out cycles. Compared to both Groups 1 and 2, the profiles here exhibit greater variation in shape and peak amplitude, suggesting more pronounced mechanical interaction and potential cumulative surface damage.

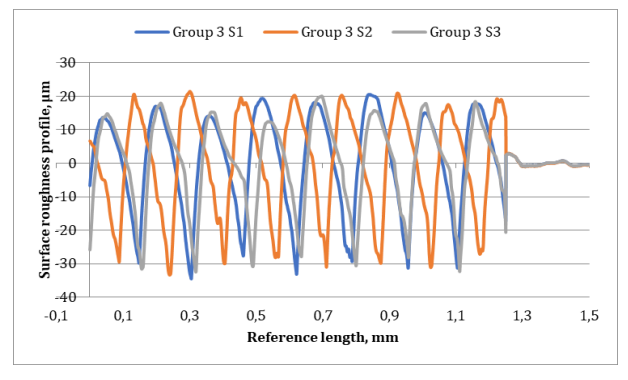


Fig. 15. Surface roughness profiles of Group 3 samples.

Sample S1 retains a regular sinusoidal pattern with peaks reaching up to +20 µm and valleys extending to -30 µm, similar to Group 1, but with slightly shortened peak spacing, possibly indicating mild compression or layer smearing due to repeated loading. Sample S2 displays the most consistent wave-like structure and relatively symmetrical peaks and valleys. This suggests stable surface interaction, where deformation occurred uniformly across the contact area during both cycles. Sample S3, however, shows irregularities and interruptions in the signal, particularly in the mid-section. The loss of periodicity and localized flattening indicates possible surface abrasion or partial tearing, likely a result of friction accumulation and plastic deformation after multiple cycles.

Figure 16 presents the distribution of maximum profile height (R_{max}) over the normalized reference length for Group 3 samples, which were subjected to two full press-fitting and pulling-out cycles. All three curves exhibit the expected descending trend, with peak values at the beginning that gradually diminish along the reference length.

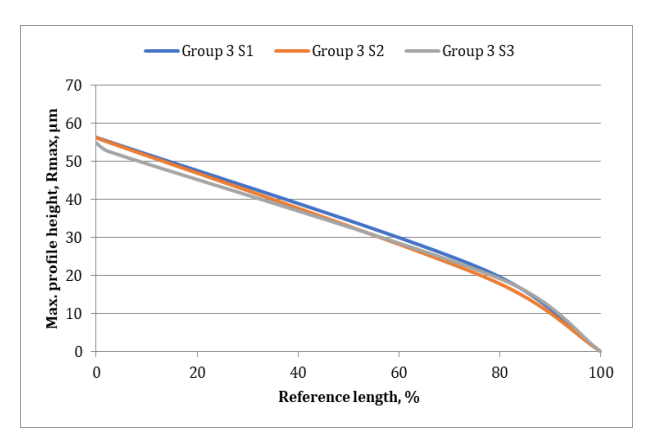


Fig. 16. Maximum profile height (R_{max}) distribution over reference length for Group 3 samples.

Sample S2 exibits the highest initial R_{max} , close to 60 µm, which may indicate slightly more aggressive surface contact or sharper asperities after the second cycle. Sample S1 maintains a moderately high starting R_{max}, while S3 starts from a lower initial value (~53 um), indicating more effective rounding or flattening of surface peaks during loading. Despite the initial variations, all three curves converge toward zero at the 100% reference length mark, confirming that no outlier peaks dominate the entire surface. The gradual and parallel decline in all three suggests consistent surface wear mechanisms across samples, with no significant deviations in deformation behaviour. These results reinforce conclusion that two mechanical cycles lead to further surface smoothing compared to Group 2, although the differences in R_{max} values among samples remain within a narrow range, indicating the reproducibility and mechanical stability of the deformation process.

6. CONCLUSION

A comparison between Group 2 and Group 3 highlights the influence of repeated mechanical loading on the performance of the press-fit joint. In Group 2, the maximum press-fitting force reached approximately 600 N, while the corresponding pulling-out force peaked at around 300 N, indicating a strong initial interference and reliable retention. In contrast, Group 3 exhibited a noticeable reduction in both press-fitting and pulling-out forces during the second cycle. The second press-fit reached only about 400 N while the second extraction force dropped below 250 N.

This corresponds to a reduction of approximately 33% in the press-fitting force and a decrease of around 17% in the pulling-out force when comparing the second cycle of Group 3 to the single cycle of Group 2. These reductions suggest that repeated assembly and disassembly lead to gradual degradation of the press-fit interface, most likely due to plastic deformation of the PET-G material or wear of the contact surfaces. The lower resistance in the second cycle implies a reduction in friction and contact pressure, confirming that repeated mechanical cycling weakens the retention capability of the joint and may compromise its long-term functional integrity.

The surface roughness analysis clearly demonstrates that mechanical cycling through press-fitting and pulling-out significantly influences the surface texture of 3D-printed PET-G housings. A clear decreasing trend in roughness with an increasing number of mechanical loading cycles is observed. Group 1 exhibits the highest Ra and Rz values, which is expected since these samples were not exposed to mechanical interactions. Group 2 shows a noticeable reduction in both parameters. while Group 3 maintains similar values to Group 2. with a slight additional decrease in Ra.

Group 2 R_{max} curves reveal reduced peak intensities compared to Group 1 and a more uniform decline pattern, supporting the hypothesis that even a single mechanical cycle contributes to the smoothing and flattening of the surface. The consistency across all three samples indicates repeatable wear mechanisms and confirms the impact of mechanical interaction on the internal geometry of the housing.

Group 3 profiles show signs of asperity rounding, supporting the hypothesis that repeated mechanical cycling alters the topographical features of the housing surface more noticeably than a single cycle. This is especially evident in the slight loss of definition in peaks and increasing asymmetry of waveforms.

Overall, the results confirm that surface roughness parameters are sensitive indicators of the extent and effects of mechanical loading. The combination of R_a and R_{max} analysis provides a comprehensive picture of how repeated interference fits impact surface integrity, potential wear behavior, and dimensional reliability in polymer-based assembly applications.

Future research should explore the effects of multiple assembly-disassembly cycles beyond two, as well as assess how different printing resolutions, filament manufacturers, slicing software, and 3D printer models influence the mechanical and surface performance of interference-fit joints. Such investigations would provide a broader understanding of the variability introduced by process parameters and material sources, and help define the robustness and applicability of the presented findings across a wider range of additive manufacturing conditions.

Acknowledgement

This paper is the result of research conducted under the author's contract No. 451-03-137/2025-03/200107, dated February 4, 2025 and scientific research work 451-03-136/2025-03/200378.

REFERENCES

- [1] L. Lopes, D. Reis, A. Paula Junior, and M. Almeida, "Influence of 3D Microstructure Pattern and Infill Density on the Mechanical and Thermal Properties of PET-G Filaments," *Polymers*, vol. 15, no. 10, p. 2268, May 2023, doi: 10.3390/polym15102268.
- [2] F. Nicita, C. D'Amico, V. Filardi, D. Spadaro, E. Aquilio, M. Mancini, et al., "Chemical-Physical Characterization of PET-G-Based Material for Orthodontic Use: Preliminary Evaluation of micro-Raman Analysis," *European Journal of Dentistry*, vol. 18, no. 1, pp. 228–235, May 2023, doi: 10.1055/s-0043-1764424.
- [3] S. V. Lakshman Sri, A. Karthick, and C. Dinesh, "Evaluation of Mechanical Properties of 3D Printed PETG and Polyamide (6) Polymers," *Chemical Physics Impact*, vol. 8, p. 100491, Jun. 2024, doi: 10.1016/j.chphi.2024.100491.
- [4] L. Marsavina, V. Dohan, and S.-V. Galatanu, "Mechanical Evaluation of Recycled PETG Filament for 3D Printing," *Frattura ed Integrità Strutturale*, vol. 18, no. 70, pp. 310–321, Sep. 2024, doi: 10.3221/IGF-ESIS.70.18.
- [5] J. D. Seno Flores, T. De Assis Augusto, D. A. Lopes Vieira Cunha, C. A. Gonçalves Beatrice, E. H. Backes, and L. C. Costa, "Sustainable polymer reclamation: recycling poly(ethylene terephthalate) glycol (PETG) for 3D printing applications," *Journal of Materials Science: Materials in Engineering*, vol. 19, no. 1, p. 16, Aug. 2024, doi: 10.1186/s40712-024-00163-x.

- [6] M.-H. Hsueh, C.-J. Lai, S.-H. Wang, Y.-S. Zeng, C.-H. Hsieh, C.-Y. Pan, et al., "Effect of Printing Parameters on the Thermal and Mechanical Properties of 3D-Printed PLA and PETG, Using Fused Deposition Modeling," *Polymers*, vol. 13, no. 11, p. 1758, May 2021, doi: 10.3390/polym13111758.
- [7] S. Milenkovic, V. Slavkovic, C. Fragassa, N. Grujovic, N. Palic, and F. Zivic, "Effect of the raster orientation on strength of the continuous fiber reinforced PVDF/PLA composites, fabricated by hand-layup and fused deposition modeling," *Composite Structures*, vol. 270, p. 114063, May 2021, doi: 10.1016/j.compstruct.2021.114063.
- [8] F. Zivic, S. Mitrovic, N. Grujovic, Z. Jovanovic, D. Dzunic, and S. Milenkovic, "The Influence of the 3D Printing Infill and Printing Direction on Friction and Wear of Polylactic Acid (PLA) under Rotational Sliding," *Journal of Friction and Wear*, vol. 42, no. 2, pp. 106– 111, Mar. 2021, doi: 10.3103/s1068366621020124.
- [9] N. Palic, V. Slavkovic, Ž. Jovanovic, F. Zivic, and N. Grujovic, "Mechanical behaviour of small load bearing structures fabricated by 3D printing," *Applied Engineering Letters*, vol. 4, pp. 88–92, 2019.
- [10] A. F. Rashed, M. N. H. Damir, A. S. Cherif, and M. A. Afifi, "Study of deformation and form error due to press-fitting a thick cylinder into a square outer housing," *Wear*, vol. 60, no. 2, pp. 339–347, May 1980, doi: 10.1016/0043-1648(80)90232-X.
- [11] A. Khubchandani, M. McCullough, and W. Deporter, "A Comparative Study of Bearing Press Fit Contact Modeling Techniques with Current Finite Element Analysis Tools," *SAE Technical Paper*, pp. 1-11, Apr. 2011, doi: 10.4271/2011-01-1049.
- [12] D. Benuzzi and G. Donzella, "Prediction of the press-fit curve in the assembly of a railway axle and wheel," *Proceedings of the Institution of Mechanical Engineers, Part F: Journal of Rail and Rapid Transit*, vol. 218, no. 1, pp. 51–65, Jan. 2004, doi: 10.1243/095440904322804439.
- [13] A. N. Natali, E. L. Carniel, and P. G. Pavan, "Investigation of viscoelastoplastic response of bone tissue in oral implants press fit process," *Journal of Biomedical Materials Research Part B: Applied Biomaterials*, vol. 91B, no. 2, pp. 868–875, Nov. 2009, doi: 10.1002/jbm.b.31469.
- [14] V. Weißmann, C. Boss, C. Schulze, H. Hansmann, and R. Bader, "Experimental Characterization of the Primary Stability of Acetabular Press-Fit Cups with Open-Porous Load-Bearing Structures on the Surface Layer," *Metals*, vol. 8, no. 10, p. 839, Oct. 2018, doi: 10.3390/met8100839.
- [15] I. Buj-Corral, A. Bagheri, and M. Sivatte-Adroer, "Effect of Printing Parameters on Dimensional Error, Surface Roughness and Porosity of FFF Printed Parts with Grid Structure," *Polymers*, vol. 13, no. 8, p. 1213, Apr. 2021, doi: 10.3390/polym13081213.

- [16] M. Altan and V. Kovan, "Printing Parameters Effect on Surface Characteristics of 3D Printed PLA Materials," *Machines. Technologies. Materials*, vol. 12, no. 7, pp. 266–269, 2018.
- [17] A. Garg, A. Bhattacharya, and A. Batish, "On Surface Finish and Dimensional Accuracy of FDM Parts after Cold Vapor Treatment," *Materials and Manufacturing Processes*, vol. 31, no. 4, pp. 522–529, Mar. 2016, doi: 10.1080/10426914.2015.1070425.
- [18] S. Djurović, D. Lazarević, M. Ivković, M. Mišić, B. Stojčetović, and Ž. Šarkoćević, "Tribological behaviour and surface roughness quality of 3D printed ABS material," *Journal of Materials and Engineering*, vol. 1, no. 3, pp. 116–120, Oct. 2023, doi: 10.61552/jme.2023.03.004.
- [19] N. Petrović, S. Milenković, Ž. Jovanović Pešić, N. Kostić, and N. Marijanović, "Determining 3D Printed Housing Diameters for Press-Fitting Standard Ball Bearings," in International Congress Motor Vehicles & Motors 2024, Kragujevac, Serbia, Oct. 10–11, 2024, pp. 379–383.
- [20] E. S. Gadelmawla, M. M. Koura, T. M. A. Maksoud, I. M. Elewa, and H. H. Soliman, "Roughness parameters," *Journal of Materials Processing*

- *Technology*, vol. 123, no. 1, pp. 133–145, Apr. 2002, doi: 10.1016/S0924-0136(02)00060-2.
- [21] B. Bhushan, "Surface Roughness Analysis and Measurement Techniques," 2001. [Online]. Available: https://api.semanticscholar.org/CorpusID:5711972.
- [22] B. You, Z. Lou, Y. Luo, Y. Xu, and X. Wang, "Prediction of Pressing Quality for Press-Fit Assembly Based on Press-Fit Curve and Maximum Press-Mounting Force," *International Journal of Aerospace Engineering*, vol. 2015, pp. 1–10, Jan. 2015, doi: 10.1155/2015/823019.
- [23] E. Dieudonné, O. Florence, N. A. Joseph, N. A. Claude Valery, N. P. Achille, and Z. Crick Nelson, "A study on the experimental investigation of low frequency vibration wave assisted disassembly of press-fit joints," *Journal of Manufacturing Processes*, vol. 49, pp. 70–81, Jan. 2020, doi: 10.1016/j.jmapro.2019.11.014.
- [24] M. Alsoufi and A. El-Sayed, "How Surface Roughness Performance of Printed Parts Manufactured by Desktop FDM 3D Printer with PLA+ is Influenced by Measuring Direction," *American Journal of Mechanical Engineering*, vol. 5, pp. 221–222, Nov. 2017, doi: 10.12691/ajme-5-5-4.